Correlation between morphology, chemical environment, and ferromagnetism in the intrinsic-vacancy dilute magnetic semiconductor Cr-doped Ga_{2}Se_{3}/Si(001)

E. N. Yitamben, T. C. Lovejoy, A. B. Pakhomov, S. M. Heald, E. Negusse, D. Arena, F. S. Ohuchi, and M. A. Olmstead

Correlation between Morphology, Chemical Environment, and Ferromagnetism in the Intrinsic-Vacancy Dilute Magnetic Semiconductor Cr-doped Ga$_2$Se$_3$/Si(001)

E. N. Yitamben,[1, 2, *] T. C. Lovejoy,[1, 2, †] A. B. Pakhomov,[2] S. M. Heald,[3] E. Negusse,[4] D. Arena,[5] F. S. Ohuchi,[6, 2] and M. A. Olmstead[1, 2]

[1]*University of Washington, Department of Physics, Box 351560, Seattle, Washington 98195, USA*

[2]*The Center for Nanotechnology, University of Washington, Box 352140, Seattle, Washington 98195, USA*

[3]*Advanced Photon Source, Argonne National Laboratory, Argonne, Illinois 60439, USA*

[4]*Department of Physics, Montana State University, Bozeman, Montana 59717, USA*

[5]*National Synchrotron Light Source, Brookhaven National Laboratory, Upton, New York 11973, USA*

[6]*University of Washington, Department of Materials Science and Engineering, Box 352120, Seattle, Washington 98195, USA*

(Dated: November 30, 2010)

Chromium-doped gallium sesquiselenide, Cr:Ga$_2$Se$_3$, is a member of a new class of dilute magnetic semiconductor exploiting intrinsic vacancies in the host material. The correlation among room-temperature ferromagnetism, surface morphology, electronic structure, chromium concentration and local chemical and structural environments in Cr:Ga$_2$Se$_3$ films grown epitaxially on silicon is investigated with magnetometry, scanning tunneling microscopy, photoemission spectroscopy and x-ray absorption spectroscopy. Inclusion of a few percent chromium in Ga$_2$Se$_3$ results in laminar, semiconducting films that are ferromagnetic at room temperature with a magnetic moment $\geq 4\mu_B$/Cr. The intrinsic-vacancy structure of defected-zinc-blende $\beta-$Ga$_2$Se$_3$ enables Cr incorporation in a locally octahedral site without disrupting long-range order, determined by x-ray absorption spectroscopy, as well as strong overlap between Cr $3d$ states and the Se $4p$ states lining the intrinsic vacancy rows, observed with photoemission. The highest magnetic moment per Cr is observed near the solubility limit of roughly one Cr per three vacancies. At higher Cr concentrations, islanded, metallic films result, with a magnetic moment that depends strongly on surface morphology. The effective valence is Cr^{3+} in laminar films, with introduction of Cr^0 upon islanding. A mechanism is proposed for laminar films whereby ordered intrinsic vacancies mediate ferromagnetism.

PACS numbers: 75.50.Pp, 75.70.-i, 79.60.-i, 78.70.Dm, 68.37.Ef, 68.55.-a

I. INTRODUCTION

Dilute magnetic semiconductor (DMS) materials, in which introduction of a few atomic percent transition metal into a non-magnetic semiconductor leads to ferromagnetic (FM) or other magnetic phenomena, are a key element in many proposed spintronic devices.[1] However, no material to date combines room-temperature ferromagnetism, semiconducting behavior and spin-polarized free carriers with silicon compatibility. Spin injection into GaAs has been demonstrated from the FM-DMS Mn-doped GaAs, but only well below room temperature.[2] High-Curie-temperature, wide-band-gap oxides and nitrides have attracted much interest since the original reports of room-temperature FM in transition-metal-doped TiO$_2$ and ZnO.[3,4] However, neither these nor other dilute wide-bandgap, room-temperature ferromagnetic (RTFM) materials have yet demonstrated clear spin polarization of carriers characteristic of true DMS, or been successfully integrated with Si, the leading candidate for spintronics due to its ubiquity, low spin-orbit interaction and long spin diffusion lengths.

There are two primary approaches to the origin of ferromagnetism in dilute magnetic semiconductors and dielectrics: carrier or defect mediated. Spin polarization of carriers in a DMS naturally accompanies FM with a carrier-mediated mechanism of ferromagnetic ordering, as formulated for Mn:GaAs.[5] In recent models of defect mediation in dilute RTFM materials, ferromagnetic ordering is acquired only in the presence of structural defects, typically having open volume character, including vacancies, grain boundaries and surfaces,[6–10] which are difficult to control reproducibly. The intrinsic vacancy structure of Ga$_2$Se$_3$, where one-third of cation sub-lattice sites are vacant and the chalcogenide lone-pair states lining vacancy rows form anisotropic band-edge states,[11,12] is intermediate between band- and defect-mediated systems, making it a promising host for RTFM DMS with enhanced propensity both for RTFM and carrier spin polarization.

This paper focuses on the correlation between magnetism and the local structural, chemical and electronic order in the silicon-compatible material Cr-doped Ga$_2$Se$_3$, which we find exhibits evidence for room temperature ferromagnetism. Chromium is a transition metal of interest for which room temperature ferromagnetism in magnetic semiconductors has been demonstrated both theoretically and experimentally in GaN,[13–16] AlN,[15,16] ZnTe,[17,18] TiO$_2$[8,19,20], and ZnO.[9] Ga$_2$Se$_3$ is a III-VI semiconductor with a band gap of about 2.5 eV and is closely lattice matched to silicon ($\sim 0.1\%$ mismatch); the intrinsic cation vacancies align along [1$\bar{1}$0] directions. Our demonstrated ability to fabricate

ordered vacancy structures during epitaxial growth of Ga_2Se_3 on silicon[21] and to grow epitaxial TM-doped TiO_2 on Ga_2Se_3/Si[22] makes Ga_2Se_3 the natural choice for initial investigation.

This paper establishes correlations among chemical composition, local structure, chromium valence, surface morphology, and magnetism in epitaxial Cr-doped Ga_2Se_3 films on silicon using scanning tunneling microscopy (STM), photoemission spectroscopy, x-ray absorption spectroscopy (XAS) and magnetometry measurements. Below a solubility limit of ~ 8 atomic percent,[23] Cr incorporates uniformly into cubic Ga_2Se_3 and films remain laminar to at least 20 nm in thickness. Surprisingly, the Cr is found to occupy a locally octahedral site without long-range disruption of the defected-zincblende lattice, a situation enabled by the large intrinsic vacancy concentration; a model is proposed whereby Cr substitutes for Ga in conjunction with a rotation of bonds around a single Se. Spectroscopy reveals semiconducting films, with Cr in a 3^+ valence state interacting primarily with selenium. The magnetic moment per Cr is at or above the expected moment for Cr^{3+}, and is about 20% higher in very thin (~ 4 nm) films than in thicker ones (~ 20 nm). At higher Cr concentrations, islands populate the surface, new states are introduced at the Fermi level, and multiple Cr environments are observed. Despite these changes, high concentration films remain ferromagnetic at room temperature. The magnetic moment per Cr is highest for films just above the solubility limit, with a thin, Cr-saturated layer covering the surface, interspersed with a few Cr-rich islands. At the highest concentrations investigated, the moment is smaller for strongly islanded films grown on a pure Ga_2Se_3 buffer layer than for the flatter film obtained when the growth order is reversed (pure Ga_2Se_3 layer deposited on top of Cr-doped Ga_2Se_3.)

II. EXPERIMENT

Si(001) substrates were chemically cleaned to replace the commercial oxide, outgassed in ultrahigh vacuum (UHV, base pressure $< 5 \times 10^{-10}$ torr), flashed to $\sim 1200°C$ to remove the oxide from chemical treatment, and terminated with one monolayer (ML) of arsenic.[21,24] GaSe and Cr were simultaneously evaporated from two different Knudsen cells. GaSe was evaporated at a rate of ~ 4.0 Å/min as measured by a quartz crystal microbalance (QCM). Previous studies have shown that $\sim 1/3$ monolayer of Ga_2Se_3 is deposited on Si(001):As per monolayer of GaSe flux;[21] we find the sticking coefficient increases with the addition of Cr and as the film becomes thicker. For the laminar thin films with total GaSe + Cr accumulation on the QCM of $4 - 7$ nm, *e.g.* Fig. 1(c,d,e,g), x-ray photoemission spectroscopy (XPS) showed the resultant films (doped + undoped layers) to be $2 - 3$ nm thick. All samples were deposited at a substrate temperature between 475 and 500 °C, with a constant GaSe flux, with the only variation being the timing and amount of the Cr co-deposition. Data for films with Cr concentration $\leq 6\%$ in Fig. 6 were obtained from a sample where the Cr concentration was varied uniformly with position by repeated passes of a shutter across the path of the Cr flux. The incident flux has equal atomic percent Ga and Se, but the resultant structure on Si(001) is cubic Ga_2Se_3 and not hexagonal GaSe. For flat, $3 - 4$ nm films with 6% Cr in the incident flux, XPS showed a Ga : Se ratio 2/3 that of GaSe-bilayer terminated Si(111),[25] low-energy electron diffraction (LEED) showed a square pattern similar to that for pure Ga_2Se_3,[12] and x-ray diffraction showed only peaks associated with Ga_2Se_3 or Si. Below, films are labeled by the atomic percent Cr in the incident flux of (Cr + GaSe), although the actual Cr concentration in the film is likely to be different. Scaling from Hartree-Fock cross sections,[26] XPS measurements on a flat, 3 nm film with 6 atomic percent Cr in the incident flux had a Cr : (Cr + Ga) ratio of $x = 0.08$.

Chromium concentrations were varied up to 16 atomic percent in the incident flux (measured with the QCM). Two different growth sequences were used: 1) co-deposition of Cr and GaSe on the Si(001):As substrate, followed by an overlayer of pure Ga_2Se_3, and 2) deposition of a pure Ga_2Se_3 buffer layer, followed by co-deposition of a doped layer. We will use the notation developed in reference 23: A/B% to denote the nominal Cr concentrations in each layer, e.g. 0/8% for a film using growth sequence 2, with an undoped buffer layer followed by a Cr-doped film with 8% Cr in the incident flux, and 8/0% for the reverse, with growth sequence 1. Photoemission shows some diffusion of Cr into the pure overlayer for $x/0\%$ films although there was not clear surface segregation. Previous work has shown that some As diffuses into the Ga_2Se_3 film, occupying Se sites.[27]

Films were grown and investigated under UHV for STM and XPS (in Seattle) and for high resolution photoemission spectroscopy (at the Advanced Light Source); they were transported in air for magnetometry measurement and/or x-ray diffraction in Seattle and for x-ray absorption measurements at the Advanced Light Source (ALS), Advanced Photon Source (APS) and/or National Synchrotron Light Source (NSLS). Magnetic properties were measured using a Quantum Design MPMS-5S superconducting quantum interference device magnetometer (SQuID) to 10^{-7} emu sensitivity with the field along the sample normal. X-ray diffraction was performed on a Bruker D5000 with Cu K_α radiation. Some of these films were capped with arsenic for magnetic studies.

Ex-situ K-edge x-ray absorption near-edge spectroscopy (XANES) and extended x-ray absorption fine structure (EXAFS) were performed at the APS (Argonne National Laboratory) using PNC/XOR-CAT beamline 20BM. Samples were mounted on spinners and rotated about the sample normal at a few hertz, while linearly polarized x-rays near the plane of the sample hit the surface at grazing incidence, to minimize Bragg diffraction. *Ex-situ* L-edge x-ray

absorption was performed at the NSLS (Brookhaven National Laboratory) using beamline U4B, measured in total electron yield (TEY) mode.

III. RESULTS

A. Surface Morphology and Crystal Structure

A detailed study of surface morphology during the initial stages Cr-doped Ga_2Se_3 growth on Si(001):As as a function of growth sequence and Cr concentration has been presented elsewhere,[23] and is summarized for easier reference in Fig. 1. Pure Ga_2Se_3 forms ordered nanorods associated with vacancy ordering that alternate direction with each substrate atomic step [Fig. 1(a)]. At low Cr concentration, the initial surface morphology is uniform [0/3%, 0/6% and 6/0% films in Fig. 1(c, f, h)] with a local morphology similar to pure Ga_2Se_3, but with shorter nanorod structures. The morphology is essentially independent of growth sequence [Fig. 1(c,h)]. Higher resolution images also show bright spots associated with Cr states. Lightly doped Cr-doped Ga_2Se_3/Si(001) maintains a cubic morphology up to at least ~ 24 nm thick [0/5% and 5/0% in Fig. 1(b,g)], independent of the growth sequence. No islands are observed, and the nanorods are thicker, longer, and taller than for thinner films at similar concentrations [Fig. 1(c,h)], and about 40% longer and 6 times wider than nanorods on thin pure Ga_2Se_3 [Fig. 1(a)]

Above a solubility limit of around 8 atomic percent, tall islands $(1-4$ nm) nucleate, frequently surrounded by ~ 1 nm deep trenches [0/9% and 0/16% in Fig. 1(i,j)], occupying most of the film volume by 16% Cr, and the terrace regions between the islands no longer exhibit the nanorod structure. The islands are smaller after coverage by pure Ga_2Se_3 [9/0% and 16/0% in Fig. 1(d,e)], and nanorods are observed in the terrace region for the 9/0% film, which is just above the solubility limit. Scanning Auger microscopy (SAM) reveals the islands are chromium-rich relative to the terrace regions.[23]

X-ray diffraction (XRD) from a nominally 5 nm thick film similar to that in Fig. 1(h) showed only peaks overlapping those of the Si substrate plus the zincblende [002] reflection. XRD from a thicker film, similar to that in Fig. 1(b), showed polycrystalline orthorhombic gallium in addition to defected zinbcblende Ga_2Se_3, indicating excess Ga likely forms droplets on the surface that are sufficiently widely spaced not to be observed in the few square microns investigated with STM. Fitting the [002] reflection for the thinner film showed the lattice constant to be 5.432 Å, while it was 5.424 Å in the thicker film. A similar thin film with no Cr exhibited a lattice constant 5.436 Å, while the Si substrate (measured with Cu K_β to avoid saturating the detector) lattice constant was 5.430 Å. No [002] peak was observed in a region of the sample that had been shielded during growth (i.e., bare Si).

The local Cr structural environment in laminar films was investigated with X-ray absorption spectroscopy at the Cr K-edge (Fig. 2). Comparison of the near-edge structure to relevant standards [Fig. 2(a)] indicates the line shape and edge energy are closest to those for CrSe, with a small oxide component apparent at higher energies in this air-exposed film (solid line is a linear combination of the CrSe (80%) and Cr_2O_3 (20%) standards). Surprisingly, no "pre-edge" peak is seen (c.f. Na_2CrO_4), indicating that Cr is not in a tetrahedral (non-centrosymmetric) local environment.

The extended x-ray absorption fine structure (EXAFS) gives additional information about the local Cr environment. The data are not consistent with substitutional Cr_{Ga} or Cr_V, but rather fit well to six Se neighbors at a distance of 2.56 ± 0.07 Å using the code FEFF 8.[28] The fits in Figs. 2(b,c,d) are for the bulk compound $Cr_{0.8}Ga_{1.2}Se_3$ (dotted, model B, based on structure in ref. 34) and the model shown in Fig. 8(d) (solid, model A), both including a surface oxide component with bond lengths of $2.0-2.1$ Å. The Ga K-edge (not shown) fits very well to pure Ga_2Se_3, with about 20% in Ga_2O_3. The Ga-Se first nearest neighbor bond length is found to be 2.42 ± 0.06 Å, equal to that reported for EXAFS of bulk Ga_2Se_3.[29]

B. Magnetic Properties

Magnetometry measurements on a series of Cr-doped Ga_2Se_3 films with $6-16\%$ Cr, with or without an undoped buffer or capping layer of pure Ga_2Se_3 or a capping layer of arsenic, all showed room temperature ferromagnetism, with a saturation moment $3.5-9$ μ_B/Cr and a coercive field of $100-200$ Oe. Narrow hysteresis loops at 5 K and 300 K of a 0/6% (4/20 nm) Cr:Ga_2Se_3 film are shown in Fig. 3(a), with an expanded view for low field in Fig. 3(b) (initial ramp up from $H = 0$ omitted for clarity). The saturation moment per Cr atom at 300 K is 4 ± 0.4 μ_B, with an additional paramagnetic component below ~ 10 K; the coercive field is about 200 Oe. The magnitude of the magnetic moment was independent of whether or not an additional As or pure Ga_2Se_3 capping layer was applied in situ to reduce surface oxidation upon atmospheric exposure. For laminar, non-islanded films, the moment was not strongly dependent on growth order (0/6% $\approx$ 6/0%) and scaled roughly with thickness [Fig. 3(c)], with a saturation moment/Cr of 5.0 and 5.4 ± 0.4 μ_B for two 4 nm films, and $4.0 \pm 0.4 \mu_B$ for a 24 nm film. Moments per Cr atom were

calculated assuming unit sticking coefficient for Cr. Similar measurements on pure Ga_2Se_3 films showed no trace of ferromagnetism [Fig. 3(d)].

Fig. 4 shows the room-temperature saturation moment per Cr for several films. The largest moments are observed for films just above the solubility limit, where small islands are surrounded by thin terrace regions, with the average moment varying by 20% between similarly prepared films with morphology similar to that in Fig. 1(i); the largest values are two or more times the atomic values for Cr^{2+}, Cr^{3+} or Cr^{4+}, while the smallest are comparable to that for Cr^{2+} or Cr^{3+}. At the highest concentrations, the moment per Cr is closer to the atomic values, with a larger moment for a flatter film obtained after Ga_2Se_3 capping [Fig. 1(e)] than for the strongly islanded film imaged in Fig. 1(j).

The magnetic moment at a field $H = 100$ Oe is shown as a function of temperature in Fig. 5 for a 0/9% film during warming from 2 K to 340 K after cooling in a magnetic field (FC, solid line) and after cooling in zero field [ZFC, dashed (green) line]. A clear difference characteristic of ferromagnetism is observed up to the instrument limit of 340 K, indicating a Curie temperature above 340 K. A paramagnetic component is also observed below ~ 10 K for this as well as all other films measured [see, *e.g.*, Fig. 3(a)].

C. Chemical Environment

The element specific chemical environment and the Cr oxidation states of Cr-doped Ga_2Se_3 were studied using high resolution photoemission spectroscopy and L-edge x-ray absorption. Fig. 6 shows valence band, Se $3d$, and Cr $2p$ photoemission for thin Cr-doped films deposited on a pure buffer layer (photoemission attenuation data indicates ~ 2 nm doped film on a 0.6 nm buffer layer). Qualitatively similar results were obtained for the inverse growth sequence (not shown). The pure through 0/6% data were obtained from a single sample with varying Cr concentration, while the higher concentration samples were separate growths.

Below the Cr solubility limit, the valence band maximum remains a few tenths of an eV below the Fermi level, indicating that the film remains a weakly-*p*-type semiconductor, and neither the valence band nor core-levels shift more than 0.1 eV, irrespective of the growth sequence (Fig. 6). Addition of chromium introduces a new state near the top of the valence band [Fig. 6(a)], with a maximum ~ 1.8 eV below the Fermi level. At higher Cr concentration (0/12% and 0/16%), the peak at -1.8 eV grows more pronounced, and new states appear in the Ga_2Se_3 band gap with a clear metallic Fermi edge. Angle-resolved measurements (not shown) reveal that these new states are distributed uniformly across the Brillouin zone. The features associated with the Ga_2Se_3 valence band (peaks near -3.0 and -7.3 eV) shift by ~ 0.5 eV to higher binding energy relative to the low-concentration films.

Examination of core level emission from Ga, Se, Si and As reveals that Se is most affected by the addition of Cr into the lattice, with Ga, Si and As showing only small binding energy shifts with constant lineshape. Fig. 6(b) shows the evolution of the Se $3d$ peak from pure Ga_2Se_3 to 16% Cr. The two spin-orbit-split $3d$ components in pure Ga_2Se_3 arise from Se adjacent to 1 vacancy (main peak, Se_{1V}), and Se adjacent to 2 vacancies (right shoulder, Se_{2V}).[21] Below the solubility limit, the Se_{2V} component decreases with increasing Cr concentration while Se_{1V} increases. At higher concentrations, the peak broadens, and multiple Se sites are present; the overall peak also shifts ~ 0.5 eV to higher binding energy.

The Cr $2p$ lineshape yields information about both local environment and oxidation state. Fig. 6(c) shows the evolution of the Cr $2p$ emission with increasing Cr concentration. At low concentration, the multiplet lineshape is similar to that in Cr_2O_3,[30] consistent with Cr^{3+} in an octahedral environment. At higher Cr concentration, where the films are islanded, a lineshape with a mixture of Cr^0 and higher oxidation states is observed.

Further information about the Cr valence may be obtained from x-ray absorption spectroscopy at the L-edge ($2p-3d$ transition). Fig. 7 shows XAS spectra for ~ 24 nm thick 0/5% and 5/0% films; a reference spectrum from powdered Cr_2O_3 is also shown. The morphology of these thicker films is shown in Figs. 1(b) and (g).

The peak positions labeled A, B, C, and D reflect the relative strength of the atomic and crystal field interactions for a given atomic multiplet.[31,32] The lineshape for both the 0/5% and 5/0% films shows clear correlation with the octahedral Cr^{3+} of the Cr_2O_3 reference spectrum, with the position of peaks A, B, and C occurring at the same energies, i.e. $578.3, 579.5$, and 580.4 eV; the D peak is not as clear as all others, and occurs around at 582.2 eV. The intensity ratios are different, however, between the Cr_2O_3 reference and the Cr:Ga_2Se_3 films, with the A peak having a much larger intensity in the film. The 0/5% film has a slightly larger B/A intensity ratio than the 5/0% film. The B/A ratio was also seen to increase with time at low temperature as oxygen adsorbed on the film, as does the structure on the low-energy side of the edge (seen clearly in the Cr_2O_3 spectrum) associated with extended fine structure from the oxygen K-edge.

IV. DISCUSSION

The results described above may be summarized as follows. Cr-doped Ga_2Se_3 films grown epitaxially on Si(001):As are ferromagnetic at room temperature for a large range of Cr concentrations and growth morphologies. Below a solubility limit of $\sim 8\%$, Cr incorporates into the Ga_2Se_3 lattice, maintaining the same overall defected zincblende structure. The films remain semiconducting, with Cr-induced states overlapping the Ga_2Se_3 valence maximum. The Cr $2p$ multiplet structure in both photoemission and absorption is similar to octahedral Cr^{3+} in Cr_2O_3, though with differences in relative intensity and crystal field splitting. K-edge XANES shows the Cr is in a locally-centrosymmetric environment with an edge energy close to that for CrSe, while EXAFS shows the Cr to be in an octahedral local environment rather than substitutional on the lattice. The Cr interacts strongly with Se, with a reduction in the Se component associated with the states that published density functional calculations[11] indicate form the valence band maximum (VBM), namely Se bonded to 2 Ga, adjacent to 2 vacancies, and an increase in Cr-related states near the VBM. The magnetic moment per Cr atom in laminar films is $4-5\mu_B$, higher for thinner and/or islanded films; an additional paramagnetic component is observed below 10 K. At higher Cr concentrations, Cr-rich[23] islands precipitate during growth. These films are metallic, with both Cr and Se occupying multiple local environments, including Cr^0. The ferromagnetism in these islanded films depends on morphology, with the largest atomic moments observed for films just above the solubility limit. The ferromagnetic transition temperature is above the instrumental limit of 340 K. These results, as well as their implications for ferromagnetic mechanisms in $Cr:Ga_2Se_3$ are discussed more fully below.

A. Structure

Structural measurements, including scanning tunneling microscopy, low energy electron diffraction, x-ray diffraction, and Ga or Se XAFS, show laminar films below the solubility limit with a similar overall structure to pure Ga_2Se_3. The measured lattice constant from the zincblende [002] reflection (which is forbidden in bulk Si, and hence accessible to analysis in these ultrathin epitaxial films), indicates a slight tetragonal distortion in the thinnest film measured, which relaxes towards the bulk Ga_2Se_3 value as the film grows. Polycrystalline Ga diffraction observed for a thicker film is likely due to use of a GaSe source material without excess Se. The cubic crystal structure forces growth of Ga_2Se_3, with excess Ga migrating to large Ga droplets. We observed such droplets with scanning electron microscopy on a Mn-doped Ga_2Se_3 sample grown under similar conditions. We propose that introducing additional Se during growth will likely improve the quality of the Ga_2Se_3 films.

The absence of a pre-edge peak in Cr K-edge spectrum demonstrates that Cr does not substitute on a tetrahedral Ga or vacancy site, as it does in $Cr:GaN^{33}$ or $Cr:ZnTe,^{18}$ and the energy of the edge is consistent with a formal valence of Cr^{2+} (as in CrSe) and/or Cr^{3+} (with Se neighbors screening more efficiently than oxygen). The Cr $2p$ absorption (Fig. 7) and emission [Fig. 6(c)] multiplet structure, as well as the maintenance of semiconducting band structure up to at least 6% Cr [Fig. 6(a)] indicate that electronically Cr^{3+} is replacing Ga^{3+}.

In bulk $(Ga,Cr)_2Se_3$ compounds, Cr is in an octahedral environment while Ga is in a tetrahedral environment.[34–37] In a perfect zincblende lattice, there is no locally octahedral site: the octahedral holes of the anion sublattice are tetrahedral holes in the cation sublattice, and vice versa. In Ga_2Se_3, however, one third of the Se-sublattice octahedral holes are adjacent to two Ga atoms and two vacancies [Fig. 8(a)]. If Cr replaces one of these Ga atoms [Fig. 8(b)], the isoelectronic Cr^{3+} can obtain its preferred octahedral environment by shifting to the Se octahedral hole [Fig. 8(c)] while the only remaining adjacent Ga shifts to a neighboring vacant cation site [Fig. 8(d)]. This simple rotation around a single Se atom changes the nature of 3 vacancies (1 filled by the shifted Ga and 2 now adjacent to Cr) and leaves the Se sublattice intact. A fit of our EXAFS data to this model [Fig. 2(b), solid (model A)] finds a nearest-neighbor bond length of 2.55 ± 0.07 Å, indicating the Se atoms contract locally towards the Cr from their ideal positions 2.70 Å away, and is a slightly better fit to the data than was the $Cr_{0.8}Ga_{1.2}Se_3$ local structure (model B). The altered vacancy structure explains the observed reduction in the Se_{2V} component of the Se $3d$ with increasing Cr concentration [Fig. 6(b)], as well as both the reduction in the aspect ratio of the vacancy-induced surface nanoridges and the solubility limit of about 1 Cr per $3-4$ intrinsic vacancies (Fig. 1).

B. Magnetism

The observed magnetic moment per Cr is in general larger than that expected for isolated Cr spins; for the thickest film investigated, it roughly equals that expected if all Cr^{3+} are participating in ferromagnetism. This indicates magnetic activation of a significant fraction (if not all) the deposited Cr and, in the thinner and islanded films, some

polarization of the host lattice. The size of the magnetic signal in islanded films requires that all the Cr participate in ferromagnetism, including both islands and terraces. This indicates the new metallic phase in the islands is also ferromagnetic. The peak moment per Cr is for thin films near the solubility limit, which is about 1 Cr per three intrinsic vacancies. At this concentration, the local Cr environment is similar to that in rutile CrO_2, which is a strong ferromagnet, except with Se neighbors instead of oxygen.

Of the potential impurity phases, most are antiferromagnetic, including CrSe,[38] Cr_2O_3,[39] Cr metal,[40] CrGa,[41] and CrAs,[42] while $CrSi_2$ is diamagnetic.[46] Zincblende CrSe is theoretically predicted to be a ferromagnetic half-metal,[43] and zincblende CrAs is a half-metallic room-temperature ferromagnet,[44,45] making them potential ferromagnetic impurity phases, but that is inconsistent with the absence of states near the Fermi level in laminar films. The ferromagnetic, higher oxidation state CrO_2 is extremely unlikely under our growth conditions, and is inconsistent with the XAFS data: the Cr K-edge spectra indicate oxide bond lengths 10% longer than those of CrO_2, but consistent with Cr_2O_3, and an oxide fraction too small to account for the measured signal. Our growth conditions result in a single ML of As on the substrate, and the As is fully pumped out of the UHV system before Ga_2Se_3 deposition. The thickest film contains about 7 ML of Cr, so it is not possible for the entire signal to come from CrAs. It is possible, however, that the extra paramagnetic contribution at low temperatures, as well as the increased moment per Cr in thinner films, may be associated with As interdiffusion into the film. Unfortunately, growth of Ga_2Se_3 on Si(001) without As-termination results in amorphous films due to Si–Se reactions,[24] making it difficult to test this hypothesis. Another potential source of increased moment is polarization of surface or interface states through superexchange, as proposed to explain anomalously high moments in thin films of Cr-doped ZnO.[9]

C. Electronic Structure

Information on the energy of electronic states near the Fermi level deduced from the photoemission and x-ray absorption results of Figs. 6 and 7 is summarized in Fig. 9. New states associated with addition of Cr to the lattice initially appear at the valence band maximum, which is known to arise from Se lone pairs on Se_{2V} atoms lining the vacancy rows.[11,12] A change in the local environment of the Se_{2V} atoms is also evidenced by the reduction in the Se $3d$ core level emission associated with Se_{2V}. Given the octahedral environment deduced from the K-edge x-ray absorption, the t_{2g} triplet should have the lowest energy of the crystal-field-split $3d$ states; from the apparent $3d^3$ valence from the L-edge multiplet structure, we infer that the t_{2g} states are the new occupied states 1.7 eV below the Fermi level, and that the e_g states must be above the Fermi level.

At higher Cr concentrations (islanded films), these states are occupied, as reflected both by a change in the Cr $2p$ multiplet structure and new occupied states introduced through the gap up to the Fermi level. The entire band structure shifts down by about 0.5 eV as the Fermi level moves up through these Cr states. This is consistent with Cr no longer substituting as Cr^{3+} replacing Ga^{3+}, but rather adding Cr^0 to the lattice. The Cr and Se lineshapes also broaden significantly above the Cr solubility limit, consistent with a new, metallic phase in the islands. The islands were previously reported both to be Cr-rich and to have facet angles not expected for Ga_2Se_3.[23] We thus propose the islands, and possibly also the Cr-saturated terrace regions between them, are a metallic Cr-Ga-Se phase, with a different local environment for both the Se and Cr from that in laminar, lower-Cr-concentration films.

For the L-edge XAS, the difference between the two growth sequences can be seen in the intensity of the B/A ratio which is probably due to the exposure of the Cr-doped layer to oxygen. The center of gravity (CG), which characterizes the energies of the empty 3d electronic states for Cr-doped samples is 578.3 eV regardless of whether there is a buffer layer or not. The assignment to Cr^{3+}, however, is not unique. A comparison of our peaks to CrF_2[31] also reveals a clear similitude with Cr in a d^4 environment consistent with Cr^{2+}, when the ligand field parameters are varied. The 1.2 eV value of the crystal field splitting between the e_g and t_{2g} orbitals, deduced from our data is also similar to the value of 1.1 eV in CrF_2 and totally different from that of Cr_2O_3 for which it is 2.2 eV.[31]

D. Ferromagnetic Mechanisms at Low Concentrations

Our initial choice of the material for this new type of DMS was based on compatibility with silicon and empirical considerations regarding the role of defects in dilute RTFM wide-bandgap materials. With the information on the electronic bands and structure of Cr:Ga_2Se_3 described above, we can now discuss a possible origin of FM ordering in this material, at least in laminar films. A semi-quantitative polaronic model proposed by Coey and collaborators[6] is frequently invoked in discussions of RTFM mechanisms in oxides. While the original model was formulated for n-type oxides, where donors are associated with oxygen vacancies, we can adopt it for the p-type case, as both the defect states (acceptors) and the magnetic impurity states in Cr:Ga_2Se_3 are located close to the valence band maximum. The geometric conditions of ferromagnetism (magnetic impurity concentration below the percolation threshold, and

magnetic polaron or other defect concentration above percolation)[6] are likely satisfied in our films, with roughly 1 Cr per 3 or 4 vacancies and 10 Se. To obtain high Curie temperature, a high degree of hybridization of the Cr d-states with the defect states (acceptors in our case) is required; this condition is also satisfied in Cr:Ga$_2$Se$_3$. The Cr-induced states at the top of the valence band [Fig. 6(a)] overlap the Se lone-pair states lining the vacancy rows,[12] suggesting strong hybridization between the Cr t_{2g} and Se s,p states. In this p-type material, long-range conduction is expected along the vacancy rows, although these bands are disrupted by the Cr-induced defects. This suggests a model similar to that proposed by Coey et al.[6] for indirect exchange, which will also result in spin polarization of carriers.

V.   CONCLUSION

In conclusion, there is a strong correlation between magnetism, chemical composition, surface morphology, and film thickness in Cr-doped Ga$_2$Se$_3$. Below 6%, thick films are laminar, semiconducting, and a magnetic moment of $\sim 4\mu_B$ per Cr, with a larger moment for thinner films, which likely indicates surface and/or interface polarization. The intrinsic vacancies enable Cr to find an octahedral local environment, where strong overlap between Cr d-states and Se states lining the vacancy rows likely mediates the ferromagnetic interaction.

Higher Cr-concentration films have islands that introduce states at the Fermi level, show a mixture of Cr oxidation states including metallic Cr, and exhibit a magnetic moment that depends on thickness and the presence of a capping layer. The Cr $3d$ states overlap band states in the host Ga$_2$Se$_3$, with additional filling from $3d^3$ to $3d^5$ above the solubility limit in the host lattice when metallic islands form.

As a room-temperature ferromagnetic semiconductor that may be grown epitaxially on silicon, Cr-doped Ga$_2$Se$_3$ shows significant potential as a silicon-compatible dilute magnetic semiconductor. Above the solubility limit, the resultant ferromagnetic metallic phase has potential for contacts to the low-concentration material. Spin-polarized transport measurements should be carried out to fully establish this potential of Cr:Ga$_2$Se$_3$ for incorporation into spintronics devices.

* Electronic address: `yitamben@uw.edu`; Present address: Center for Nanoscale Materials, Argonne National Laboratory, Argonne, IL 60439 USA.

† Present address: Nion Corporation, Kirkland, WA

[1] S. A. Wolf, D. D. Awschalom, R. A. Buhrman, J. M. Daughton, S. von Molnár, M. L. Roukes, A. Y. Chtchelkanova, and D. M. Treger, Science **294** (2001) 1488-94.

[2] E. Johnston-Halperin, D. Lofgreen, R. K. Kawakami, D. K. Young, L. Coldren, A. C. Gossard, and D. D. Awschalom, Phys. Rev. B **65** (2002) 041306.

[3] Y. Matsumoto, M. Murakami, T. Shono, T. Hasegawa, T. Fukumura, M. Kawasaki, P. Ahmet, T. Chikyow, S. -Y. Koshihara, H. Koinuma, Science **291** (2001) 854-856.

[4] K. Ueda, H. Tabata, T. Kawai, Appl. Phys. Lett. **79** (2001) 988-990.

[5] T. Dietl, H. Ohno, F. Matsukura, J. Cibert, D. Ferrand, Science **287** (2000) 1019-1022.

[6] J. M. D. Coey, M. Venkatesan, C. B. Fitzgerald, Nature Mater. **4** (2005) 173-179.

[7] K. A. Griffin, A. B. Pakhomov, C. M. Wang, S. M. Heald, K. M. Krishnan, Phys. Rev. Lett. **94** (2005) 157204.

[8] T. C. Kaspar, S. M. Heald, C. M. Wang, J. D. Bryan, T. Droubay, V. Shutthanandan, S. Thevuthasan, D. E. McCready, A. J. Kellock, D. R. Gamelin, S. A. Chambers, Phys. Rev. Lett. **95** (2005) 217203.

[9] B. K. Roberts, A. B. Pakhomov, K. M. Krishnan, Appl. Phys. Lett. **92** (2008) 162511.

[10] A. Ney, K. Ollefs, S. Ye, T. Kammermeier, V. Ney, T. C. Kaspar, S. A. Chambers, F. Wilhelm, A. Rogalev, Phys. Rev. Lett. **100** (2008) 157201.

[11] M. Peressi, and A. Baldereschi, J. Appl. Phys. **83** (1998) 6.

[12] T. C. Lovejoy, E. N. Yitamben, T. Ohta, S. C. Fain, Jr., F. S. Ohuchi and M. A. Olmstead, Phys. Rev. B **81** (2010) 245313.

[13] M. B. Haider, R. Yang, H. Al-Brithen, C. Constantin, D. C. Ingram, A. R. Smith, G. Caruntu, C. J. O'Connor, J. of Crystal Growth **285** (2005) 300.

[14] R. K. Singh, S. Y. Wu, H. X. Liu, L. Gu, D. J. Smith, and N. Newman, Appl. Phys. Lett. 86, 012504 (2005) 20.

[15] H. X. Liu, Stephen Y. Wu, R. K. Singh, Lin Gu, N. R. Dilley, L. Montes, M. B. Simmonds, Appl. Phys. Lett. **85** (2004) 18.

[16] J. E. Medvedeva, A. J. Freeman, X. Y. Cui, C. Stampfl, and N. Newman, Phys. Rev. Lett. 94, (2005) 146602.

[17] H. Saito, V. Zayets, S. Yamagata, K. Ando, Phys. Rev. Lett. **90** (2003) 207202.

[18] M. Kobayashi, Y. Ishida, J. I. Hwang, G. S. Song, A. Fujimori, C. S. Yang, L. Lee, H-J. Lin, D. J. Huang, C. T. Chen, Y. Takeda, K. Terai, S-I. Fujimori, T. Okane, Y. Saitoh, H. Yamagami, K. Kobayashi, A. Tanaka, H. Saito, K. Ando, New J. of Phys. **10** (2008) 055011.

[19] T. C. Kaspar, T. Droubay, V. Shutthanandan, S. M. Heald, C. M. Wang, D. E. McCready, S. Thevuthasan, J. D. Bryan, D. R. Gamelin, A. J. Kellock, M. F. Toney, X. Hong, C. H. Ahn, and S. A. Chambers, Phys. Rev. B 73, 155327 (2006).

[20] L.-H. Ye and A. J. Freeman, Phys. Rev. B 73, 081304(R) (2006).

[21] Taisuke Ohta, D. A. Schmidt, Shuang Meng, A. Klust, A. Bostwick, Q. Yu, M. A. Olmstead, F. S. Ohuchi, Phys. Rev. Lett. **94** (2005) 116102.

[22] D. A. Schmidt, T. Ohta, C. -Y. Lu, A. A. Bostwick, Q. Yu, E. Rotenberg, F. S. Ohuchi, M. A. Olmstead, Appl. Phys. Lett. **88** (2006) 181903.

[23] E. N. Yitamben, T. C. Lovejoy, D. F. Paul, J. B. Callaghan, F. S. Ohuchi, M. A. Olmstead, Phys. Rev. B **80** (2009) 075314.

[24] S. Meng, Ph.D. Dissertation, Department of Physics, University of Washington (2000).

[25] S. Meng, B. R. Schroeder, and M. A. Olmstead, Phys. Rev. B **61** (2000) 7215-18.

[26] J. J. Yeh and I. Lindau, Atomic Data and Nuclear Data Tables **32** (1985) 1-155.

[27] T. Ohta, Ph.D. Dissertation, University of Washington (2004).

[28] A. L. Ankudinov, B. Ravel, J. J. Rehr, S. D. Conradson, Phys. Rev. B **58** (1998) 7565.

[29] S. Takatani, A. Nakano, K. Ogata, T. Kikawa, Jpn. J. Appl. Phys. **31** (1992) L458-60.

[30] S. A. Chambers, and T. Droubay, Phys. Rev. B **64** (2001) 075410.

[31] C. Theil, J. van Elp, and F. Folkmann, Phys. Rev. B 59 (1999) 7931.

[32] Yu. S. Dedkov, A. S. Vinogradov, M. Fonin, C. König, D. V. Vyalikh, A. B. Preobrajenski, S. A. Krasnikov, E. Yu. Kleimenov, M. A. Nesterov, U. Rüdiger, S. L. Molodtsov and G. Güntherodt, Phys. Rev. B **72** (2005) 060401 (R).

[33] J. J. Kim, H. Makino, M. Sakurai, D. C. Oh, T. Hanada, M. W. Cho, T. Yao, S. Emura, K. Kobayashi, J. Vac. Sci. Technol. B **23** (2005) 1308.

[34] I. Okonska-Kozłowska, K. Szamocka, E. Malicka, A. Waskowska, J. Heimann, T. Mydlarz, A. Gilewski, T. Gron, J. of Alloys and Compounds **366** (2004) 21-27.

[35] D. Skrzypek, I. Okonska-Kozłowska, K. Szamocka, E. Malicka, J. of Mag. and Mag. Mater. **285** (2005) 379.

[36] H. D. Lutz, B. Engelen, M. Fischer, and M. Jung, Z. Anorg. Allg. Chem. **566** (1988) 55-61.

[37] A. A. Zhukov, Ya. A. Kesler, V. F. Meshcheryakov and A. V. Rozantsev, Sov. Phys. Solid State **25** (1983) 1328.

[38] L. M. Corliss, N. Elliott, J. M. Hastings, R. L. Sass, Phys. Rev. **122** (1961) 5.

[39] B.N. Brockhouse, J. Chem. Phys. **21** (1953) 961-2.

[40] C.G. Shull and M.K. Wilkinson, Rev. Mod. Phys **25** (1953) 100-107.

[41] O. Gourdon, S. L. Budko, D. Williams, G. J. Miller, Inorg. Chemistry **43** (2004) 3210.

[42] N. Kazama and H. Watanabe, J. of the Phys. Soc. of Jpn. **30** (1971) 1319-1329; *ibid* **31** (1971) 943.

[43] Wen-Hui Xie, Ya-Qiong Xu, Bang-Gui Liu, D. G. Pettifor, Phys. Rev. Lett. **91** (2003) 037204.

[44] H. Akinaga, T. Manago, M. Shirai, Jpn. J. of Appl. Phys. **39** (11B) (2000) L1118-L1120.

[45] J. F. Bi, J. H. Zhao, J. J. Deng, Y. H. Zheng, S. S. Li, X. G. Wu, Q. J. Jia, Appl. Phys. Lett. **88** (2006) 142509.

[46] Isao J. Ohsugi, Tsutomu Kojima, Isao A. Nishida, Phys. Rev. B **42** (1990) 10761.

Figures

FIG. 1: (color online) Scanning tunneling microscopy revealing the surface morphology of (a) pure Ga_2Se_3; (b-e) pure Ga_2Se_3 overlayer deposited on Cr-doped Ga_2Se_3: (b) 5/0%, 19/4.5 nm; (c) 6/0%, 2.7/1.1 nm; (d) 9/0%, 2.8/1.3 nm; (e) 16/0%, 2.7/2.3 nm; and (f—j) Cr-doped Ga_2Se_3 deposited on a pure buffer layer: (f) 0/3%, 1.7/3.9 nm; (g) 0/5%, 4.6/19 nm; (h) 0/6%, 1.2/2.7 nm; (i) 0/9%, 1.3/4.7 nm; (j) 0/16%, 2.3/2.7 nm. All images are 200×200 nm^2 with tip voltage and current [5 V, 0.2 nA] except for (a) which is at [-5 V, 0.2 nA]. The z-range is 0.6 nm except for (j), where it is 1.2 nm. Quoted thickness is as measured by the QCM; actual thicknesses are lower.

FIG. 2: (color online) Cr interaction within the crystal lattice probed using x-ray absorption fine structure: (a) Cr K-edge XANES spectra for for 0/6% (3 nm/20 nm) Cr: Ga_2Se_3 as well as standards of CrSe, Cr metal, Cr_2O_3, CrO_2, and Na_2CrO_4; (b) k^2-weighted Fourier transform of Cr K-edge EXAFS data for 6% Cr:Ga_2Se_3 in crossed lines (+), with the fit to the data by FEFF calculations presented in solid and dotted lines comparing Model A and Model B (see text); (c) Difference spectrum for Model A and Model B; (d) imaginary part of the k^2-weighted Cr K-edge EXAFS transform for 6% Cr:Ga_2Se_3 (+) and FEFF calculations for two models (lines).

FIG. 3: (color online) a) Hysteresis loops at 5K and 300K of a 0/6% Cr-doped film (3/24 nm) up to 1.5 T with the field along the sample normal. b) Expanded view of the region (box) near the origin in (a). c) The full moment (including the diamagnetic Si substrate) and subtraction procedure for this and a thinner 0/6% film, with the net ferromagnetic moment in the inset. Lines are a linear fit to the diamagnetic contribution. d) Comparison of low-field room temperature moments for pure and 0/6% films on Si(111)

FIG. 4: Comparison of M_{sat} ($H = 1.5$ Tesla, $T = 300$ K) for different growth conditions. All except that labelled "thick" has 1.7 nm pure and $3 - 4$ nm doped layers; the thicker film was 3 nm pure/24 nm doped. Islanded films show smaller moment at same Cr concentration; thicker flat film (6% Cr) shows smaller M_{sat}/Cr than a thinner film at the same Cr concentration. The 0/9.5% film has the highest moment per Cr, at $\sim 9\mu_B$/Cr.

FIG. 5: Magnetic moment of 0/9% film upon warming from 2 K to 300 K in a magnetic field $H = 100$ Oe after being cooled in zero field (ZFC) or with the field on (FC). A paramagnetic component is observed at low temperature in addition to ferromagnetism up to the instrumental limit of 340 K

FIG. 6: (color online) Photoemission results showing the effect of the addition of Cr into lattice, with increasing Cr for: (a) valence band ($h\nu = 160$ eV, integrated over $30°$ window); (b) Se $3d$ emission ($h\nu = 160$ eV); (c) Cr 2p emission ($h\nu = 780$ eV). The shaded curves in (a) and (b) show the difference between the 0/6% and pure Ga_2Se_3. The data for 0 to 6% are from a single wedge-shaped film, and intensities may be directly compared. Data for the 12% and 16% films are scaled for comparison.

FIG. 7: Cr L-edge XAS for two different growth sequences, 0/5% and 5/0%, and Cr_2O_3 reference sample. Rise in signal at low energy for Cr_2O_3 is due to O K-edge extended fine structure.

FIG. 8: (color online) Crystal model: (a) Ga_2Se_3 supercell; (b) Cr replaces a Ga in the Ga_2Se_3 structure; (c) Cr moves to an octahedral site, leaving the previous site vacant; thus (d) causing a Ga to move to a previously vacant site.

FIG. 9: (color online) Deduced electronic structure from combined photoemission and x-ray absorption. On the left are spectra replotted from Figs. 6 and 7, including valence band photoemission (solid red and shaded Cr $3d$, 0/6% data) and x-ray absorption (dotted blue, 0/5% data), aligned by comparing the binding energy of the Cr $2p$ photoemission relative to the Fermi level. On the right, schematic electronic state locations are presented for Cr (blue) and Ga_2Se_3 (red), using the 2.5 eV band gap for bulk Ga_2Se_3 to align the Ga_2Se_3 conduction band minimum (CBM). The Cr $3d$ t_{2g} level shifts down through the Fermi level at high Cr concentration.
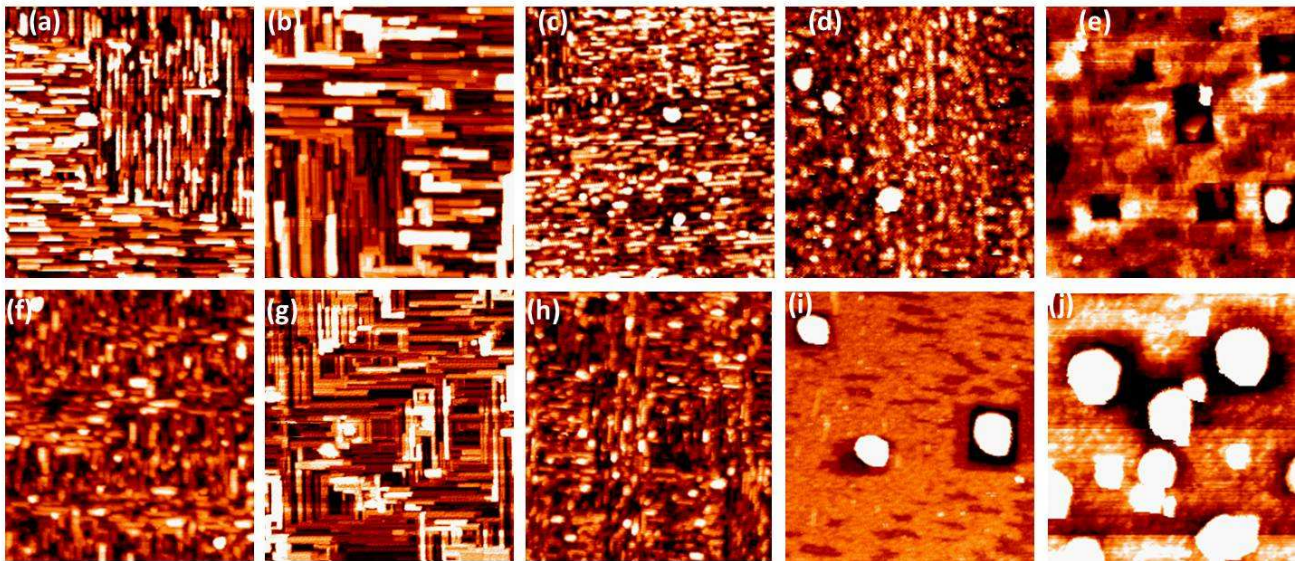
Figure 1 BU11508 30Nov2010

(a) Cr K XANES

Na₂CrO₄

CrO₂

Cr₂O₃

Cr

CrSe

Cr:Ga₂Se₃

CrSe + Cr₂O₃

Xray Absorption

Energy

(b) EXAFS   + Data
           Model A
           Model B

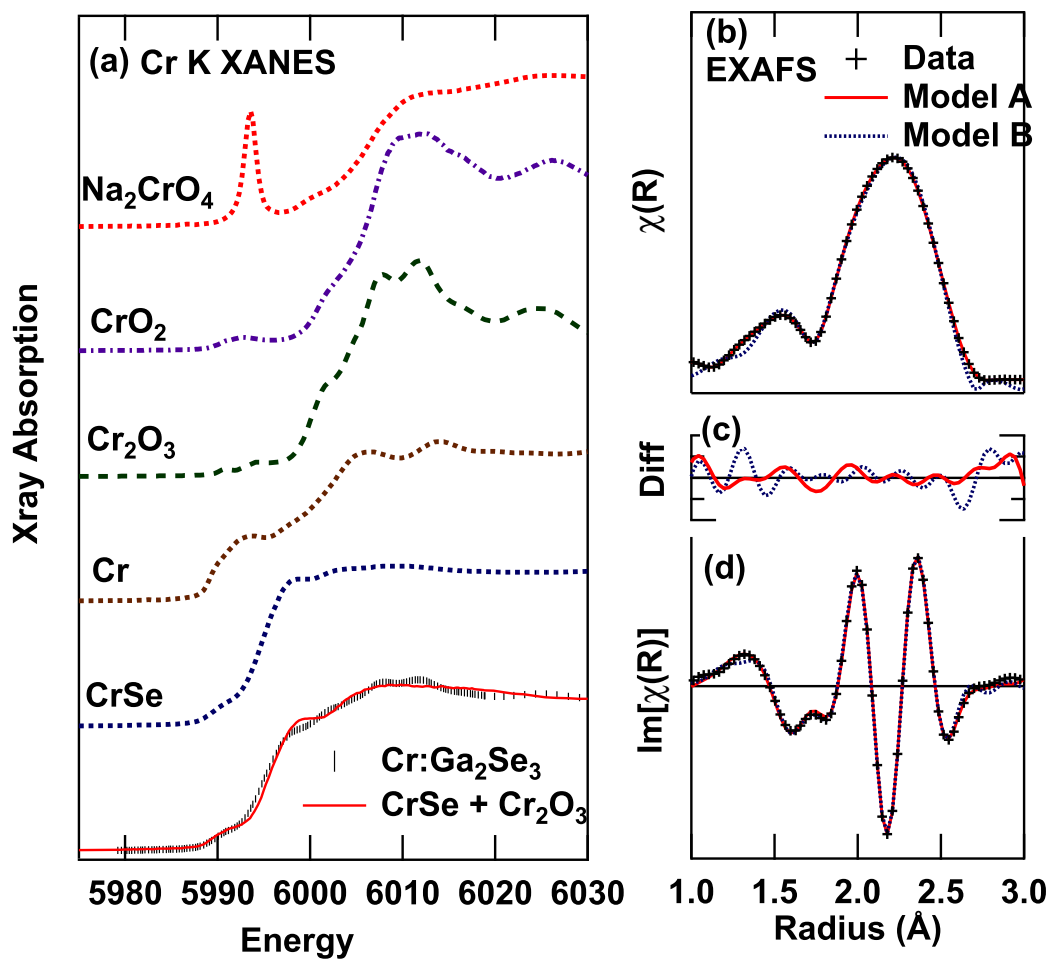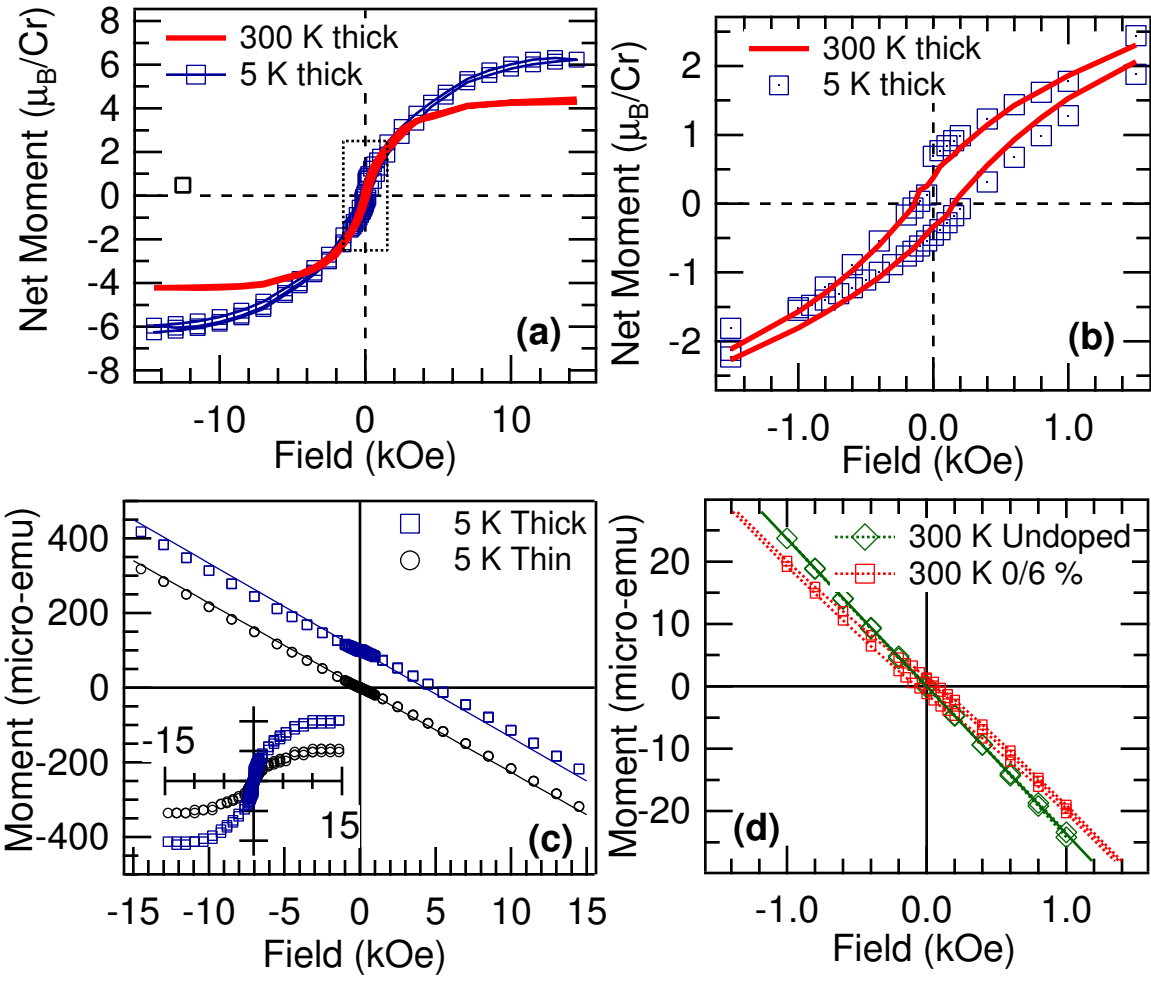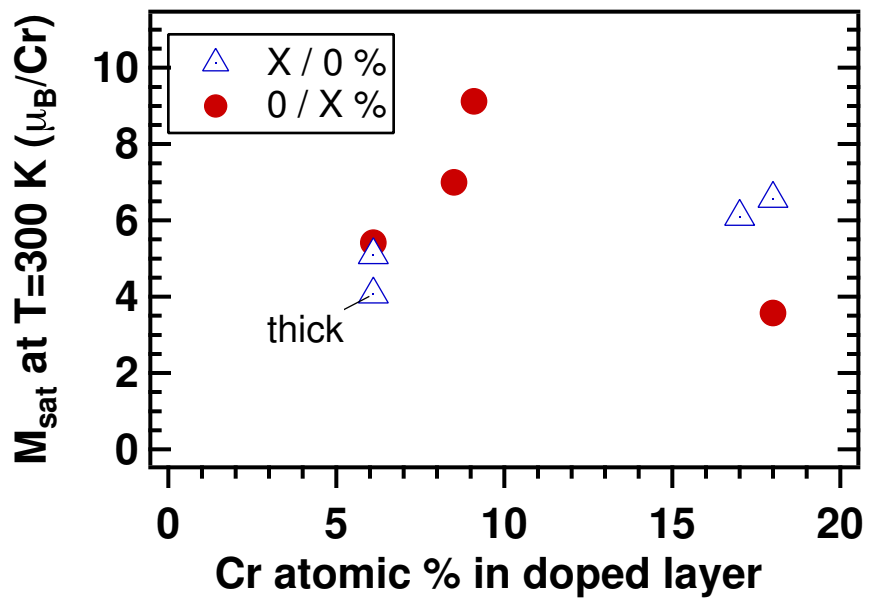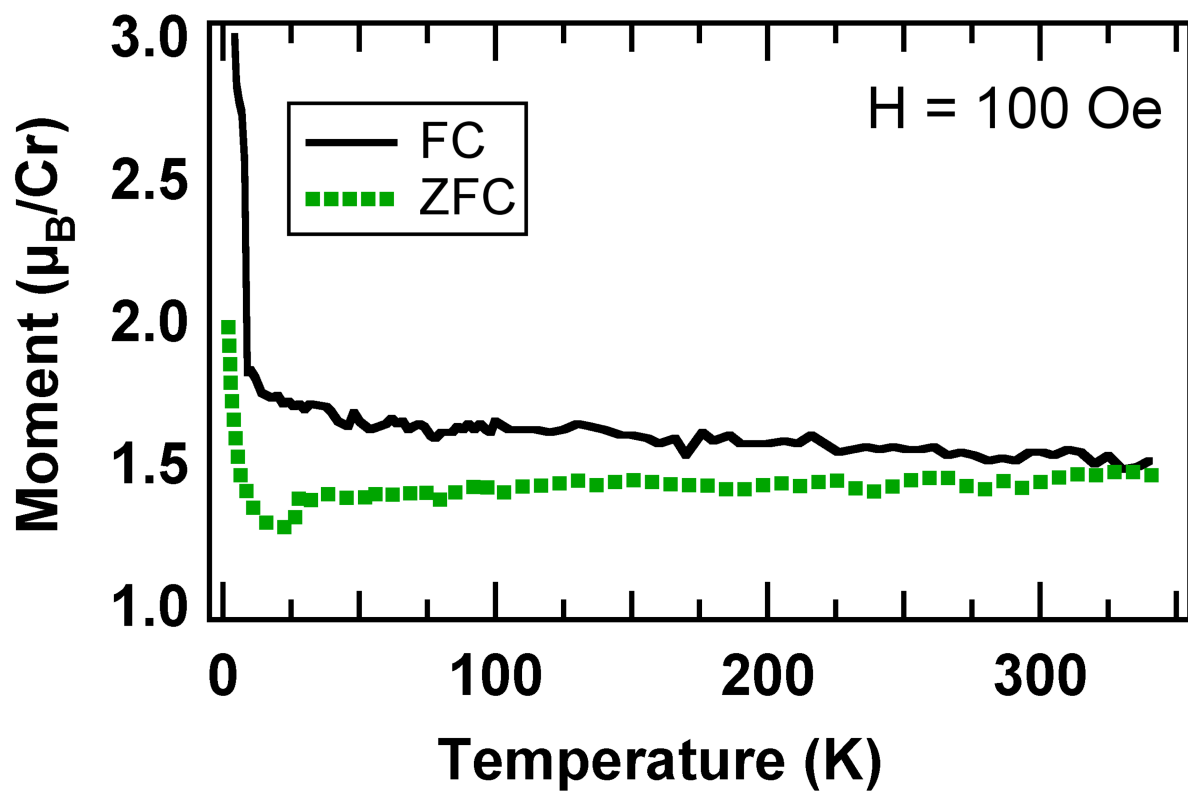χ(R)

(c) Diff

(d)

Im[χ(R)]

Radius (Å)

Figure 2   BU11508   30Nov2010

Figure 3   BU11508   30Nov2010
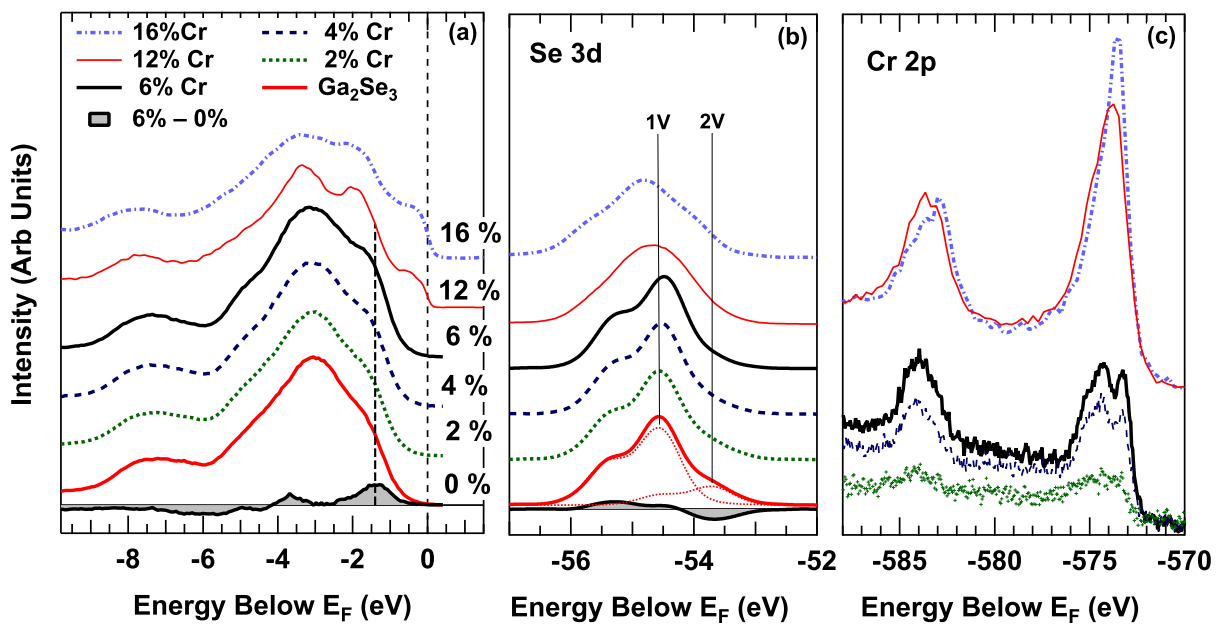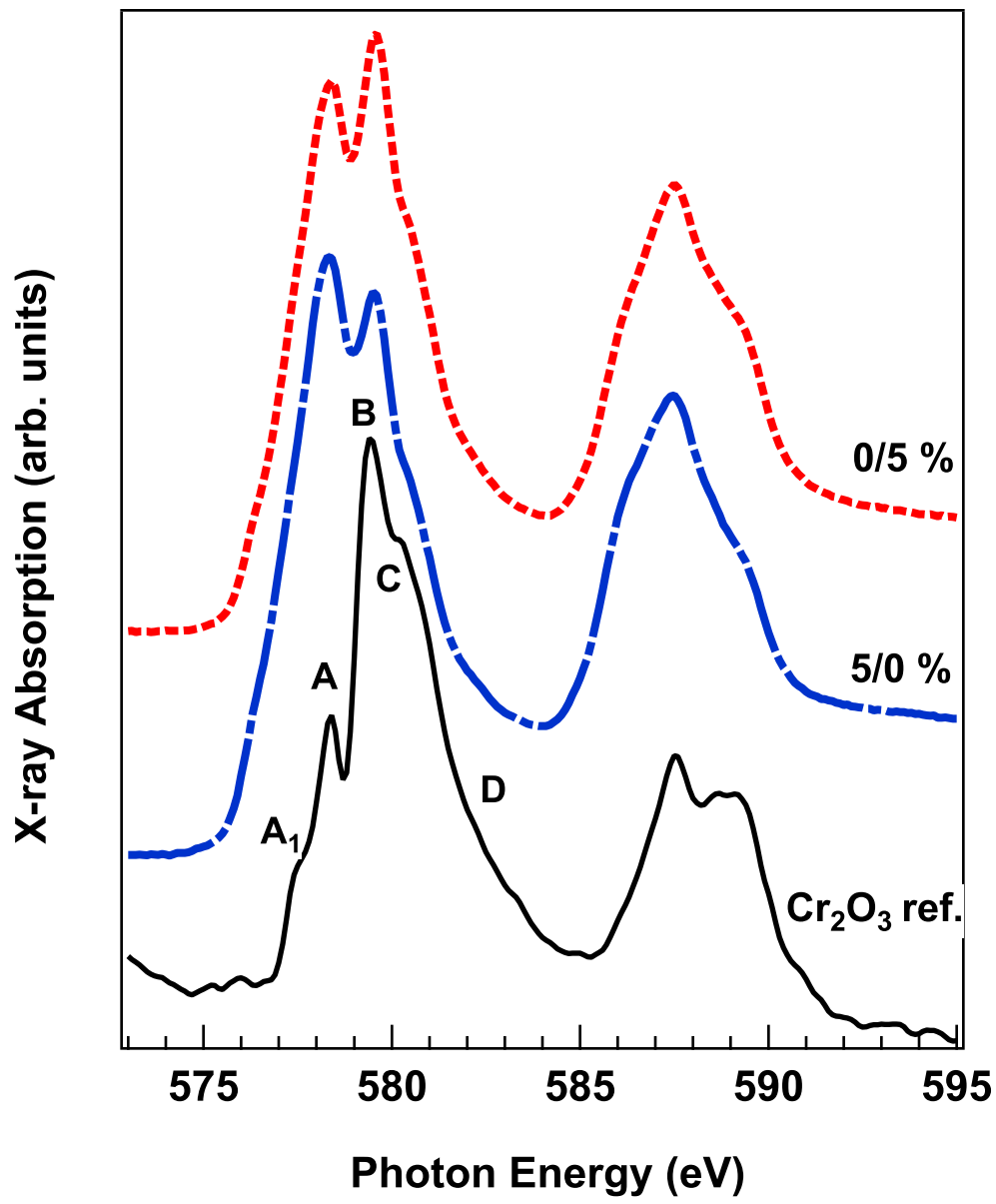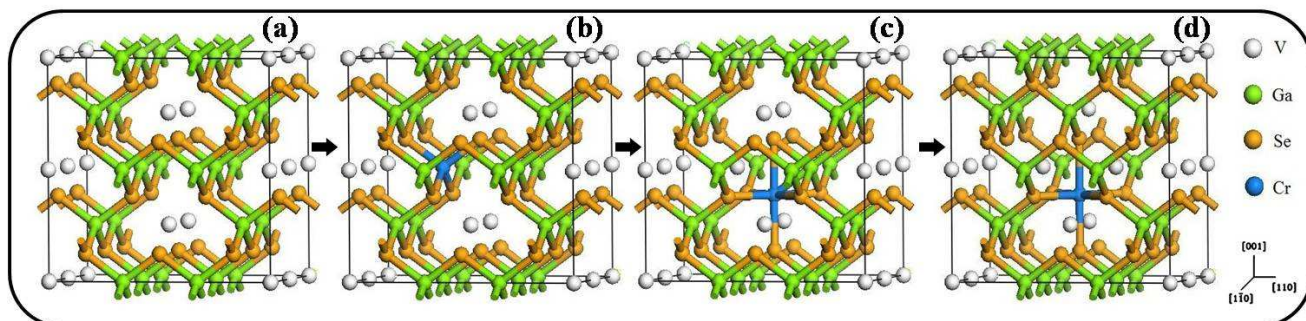
Figure 4   BU11508   30Nov2010

Figure 5   BU11508   30Nov2010

(a)

16%Cr   4% Cr
12% Cr   2% Cr
6% Cr   Ga₂Se₃
6% − 0%

16 %
12 %
6 %
4 %
2 %
0 %

Intensity (Arb Units)

Energy Below E_F (eV)

(b)

Se 3d

1V   2V

Energy Below E_F (eV)

(c)

Cr 2p

Energy Below E_F (eV)

Figure 6   BU11508   30Nov2010
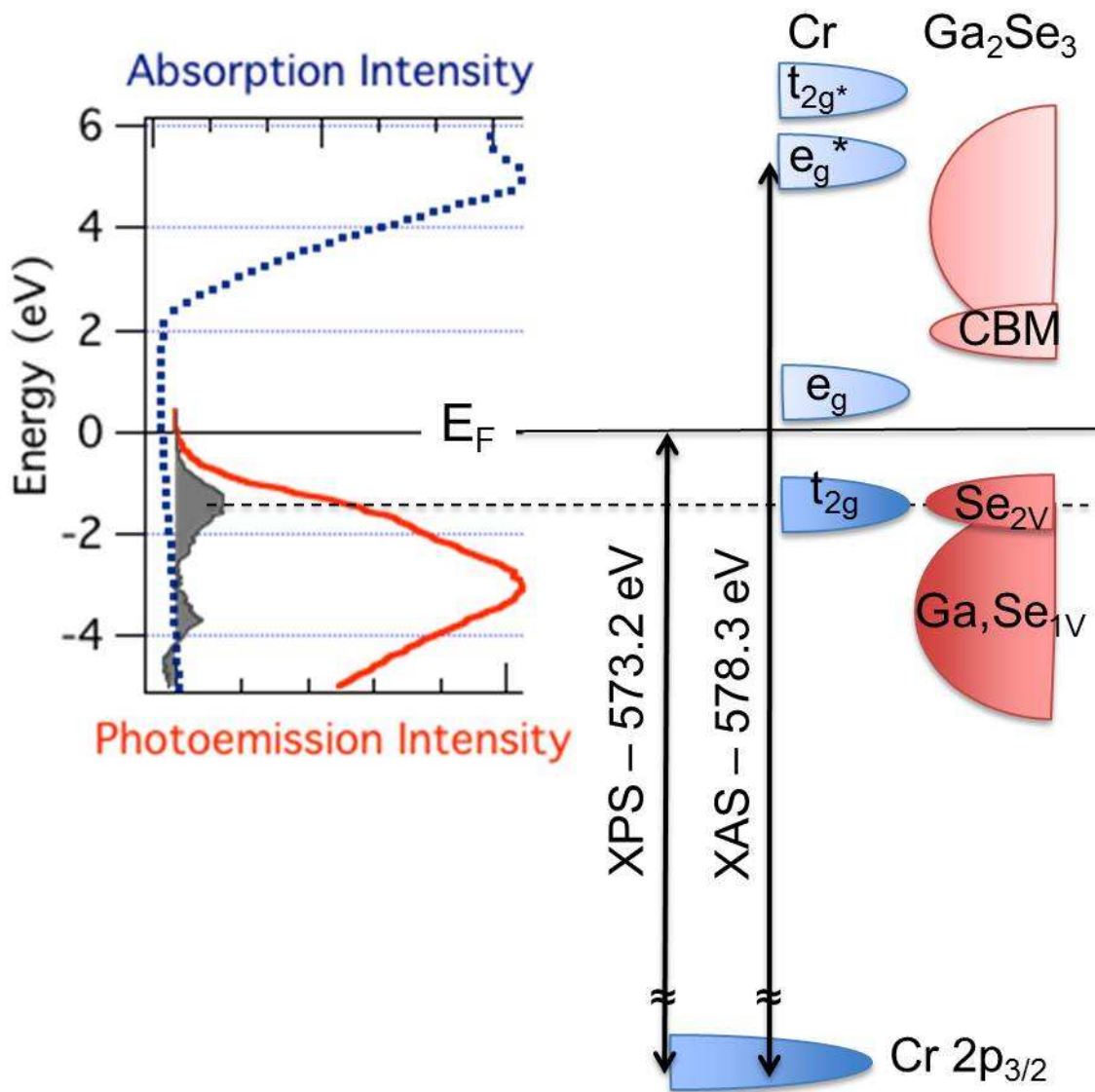
Figure 7   BU11508   30Nov2010

Figure 8   BU11508   30Nov2010

Figure 9   BU11508   30Nov2010